THREE-DIMENSIONAL NANO/MICOTEXTURE OF A LEAST ALTERED CM-RELATED CHONDRITE ASUKA 12169. A. Tsuchiyama[1,2], T. Noguci[3], M. Yasutake[1], A. Miyake[4], M. Kimura[5], A. Yamaguchi[5], N. Imae[5], K. Uesuugi[6], and A. Takeuchi[6]. [1]Research Organization of Science and Technology, Ritsumeikan University (1-1-1 Nojihigashi, Kusatsu, Shiga, 525-8577, Japan; atsuchi@fc.ritsumei.ac.jp, yasutakemasahiro.meteo@gmail.com,), [2]Guangzhou Institute of Geochemistry, Chinese Academy of Sciences (511 Kehua Street, Tianhe District, Guangzhou, GD 510640, China; atsuchi@gig.ac.cn), [3]Faculty of Arts and Science, Kyushu University (744 Motooka, Nishi-ku, Fukuoka 819-0395, Japan; tnoguchi@artsci.kyushu-u.ac.jp), [4]Division of Earth and Planetary Sciences, Graduate School of Science, Kyoto University (Kitashirakawaoiwake-cho, Sakyo-ku, Kyoto 606-8502, Japan; miya@kueps.kyoto-u.ac.jp), [5]National Institute of Polar Research (10-3 Midori-cho, Tachikawa 190-8518, Tokyo, Japan; kimura.makoto@nipr.ac.jp, yamaguch@nipr.ac.jp; imae@nipr.ac.jp), [6]Japan Synchrotron Radiation Research Institute (1-1-1 Kouto, Sayo-cho, Hyogo 679-5198, Japan; ueken@spring8.or.jp, take@spring8.or.jp)

Introduction: A few extremely primitive carbonaceous chondrites (pCCs) escaped a significant aqueous alteration (e.g., [1]-[3]). Recently, it was pointed out that Asuka (A) 12169 (CM-related) experienced very low degree of thermal metamorphism and aqueous alteration [4].

In the matrix of some pCCs, extremely pristine objects were found, such as ultra-porous lithology (UPL) as fossils of primordial ice in Acfer 094 (C-ungrouped) [5] and very carbon-rich clast as a cometary building block in LaPaz Icefiled 02342 (CR) [6]. UPLs (~10 μm in size) were first recognized by synchrotron-radiation-based X-ray computed nanotomography (SR-nanoXCT) [5]. In the analytical protocol, (1) a cross section of the meteorite was first observed by SEM, (2) regions of interest were extracted by FIB and observed using SR-nanoXCT, and then (3) sections including UPLs were sampled by FIB and analyzed using (S)TEM/EDS and nanoSIMS.

In the present study, we applied the above analytical protocol to A 12169 for 3D multiscale mineralogical and petrological examination and searching for primitive objects if present. Here, we present the 3D textures of this meteorite. SEM and TEM results are presented in [10].

Nanotomography: After FE-SEM observation of a cross section of A 12169 (5.1 mm x 3.4 mm) [10], we selected two areas and extracted blocks from these area by FIB; Sample-1 (26 x 28 x 25 μm) has the fine-grained matrix on its surface while Sample-2 (28 x 30 x 28 μm) has a chondrule, chondrule rim, and fine-grained matrix (Fig. 1 in [10]). SR-nanoCT was performed at BL47XU of SPring-8, synchrotron facility in Japan with two different methods [5]; (1) Dual-energy tomography (DET) [7]: absorption images with linear attenuation coefficient (LAC) were obtained at 7 and 7.35 keV, above and below the K-absorption edge energy of iron (7.11 keV). This enables us to discriminate Fe-rich and Fe-poor phases. The sizes of the cubic voxel are 63.9 nm and 67.6 nm at 7 and 7.35 keV, respectively. (2) Scanning-imaging X-ray microscopy (SIXM) [8]: phase contrast images with refractive index decrement (RID; refractive index is $1-\mathrm{RID}$ and RID is almost proportional to material density) were obtained at 8 keV with the voxel size of 111.06 x 111.06 x 107.7 nm. Registration of the three kinds of images for adjusting the common voxel size and direction were made by image processing. Three-color (3C) images, where R is assigned to 7.35 keV absorption images mainly corresponding to Fe content, G to phase images corresponding to density, and B to 7 keV absorption images mainly corresponding Z contrast. Many phases can be discriminated including organic materials by analyzing histograms of LACs at 7 and 7.35 keV and RID [9]. 3D distribution of specific phases was also obtained.

TEM observation was made for sections extracted from a lateral position and inside of Sample-1 [10].

Results: Representative 3C-CT images are shown in Fig. 1 and their 2D histograms in Fig. 2. Fine matrix is divided into greenish (GM) and reddish regions (RM) in both Sample-1 and -2 (Fig. 1A and C). They are mainly composed of amorphous silicate according to TEM observation [10]. GM is more abundant than RM. Chondrule rim in Sample-2 is rich in Fe sulfide nanoparticles (pink particles in Fig. 1C). In Sample-1, clasts ~5 μm in size with abundant Fe sulfide nanoparticles are seen (Fig. 1B). Peaks of GM and RM in 2D histograms are located in the left side of the forsterite-fayalite line and close to the serpentine-cronstedtite line (Figs.2A and C), showing that the amorphous silicates are hydrated. The Fe/Mg ratios of GM and RM are similar (Figs.2A and C) while the bulk density of GM (2.9~3.0 g/cm^3) is larger than RM (2.4~2.6 g/cm^3) (Figs.2B and D). The peaks of chondrule rim and FeS-rich clast in 2D histograms suggest that they are almost anhydrous and have similar Fe/Mg ratios (Figs.2A and C) while the bulk density of the rim (~3.5 g/cm^3) is lager the clast (~3.0 g/cm^3) (Figs.2B and D). Any extremally primitive objects like UPLs were not recognized. Simple statistical estimation indicates that we cannot recognize any UPL-

like material (~10 μm in size) in the CT sample if its abundance is smaller than ~0.5 vol.%.

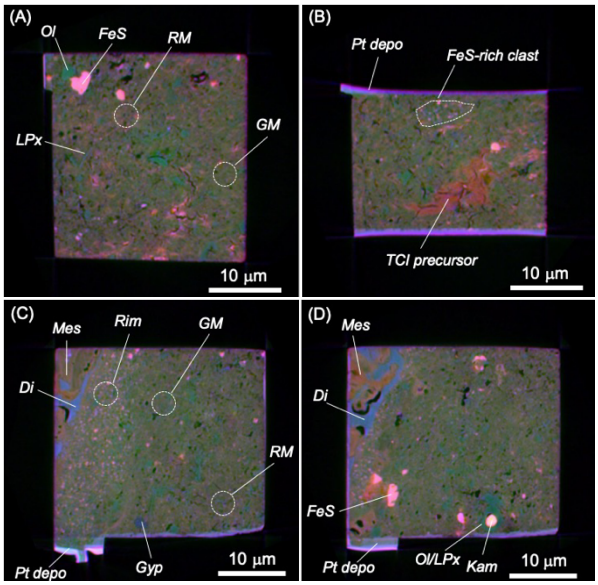

Fig. 1 Three-color CT images of A 12169. (A,B) Sample 1, (C,D) Sample-2. R: LAC (7 keV) = 0~950 cm^{-1}, G: RID (8 keV) = 0~15x10^{-6}, B: LAC (7.35 keV) = 0~450 cm^{-1}. Ol: olivine, LPx: low-Ca pyroxene, Di: diopside, Gyp: gypsum, FeS: troilite or pyrrhotite, Kam: kamacite, Mes: mesostasis, GM: greenish matrix, RM: reddish matrix, Rim: chondrule rim.

Relatively large grains of FeS (troilite or pyrrhotite) and Mg-rich olivine or low-Ca pyroxene (pink and green grains, respectively, in Fig. 1) are present in fine matrix and chondrule rim. Enstatite whiskers and platelets are present in fine matrix (e.g., LPx in Fig. 1A). TEM observation shows that at least one of them is mainly composed of low-Ca clinoenstatite elongated along the a-axis [10]. The whiskers and platelets are abundant in Sample-2 (14 crystals were recognized). Objects mainly composed of Fe-rich hydrous silicate are also observed (brown objects in Fig. 1). According to TEM observation, they may be precursors of tochilinite-cronstedtite intergrowth (TCI) (Figs 2A and B). Gypsum was found in matrix (Fig. 1C and Figs. 2C and D). Spherical objects composed of metallic core and olivine or low-Ca pyroxene mantle are also present in the matrix. The core is kamacite in Fig. 1D while core which seems to be taenite is also present in Sample-1. Abundant nanoparticles of Ni-rich metal are observed by TEM in matrix close to Sample-1 [10]. Any Ni metal and Ni monosulfide were not recognized in the CT samples with the detection limits of ~0.002, ~0.01 and 0.1 vol.% for 1, 2 and 5 μm grains, respectively. Chondrule is composed of diopside phenocryst and Fe-rich hydrous silicate (Figs. 1C and D and Figs. 2C and D).

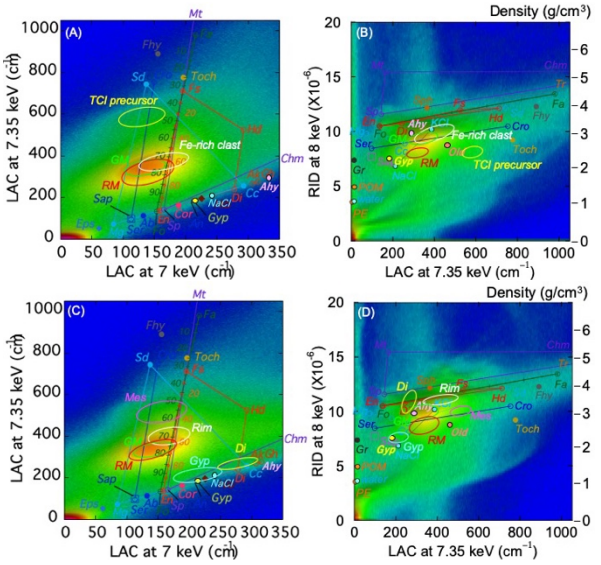

Fig. 2 2D histograms of the CT samples of A 12169 and some object peaks. (A, B): Sample 1 and (C, D): Sample-2. Abbreviations are the same as in Fig. 1.

Discussion: The texture and mineralogy of fine matrix are similar among Sample-1 and -2 while TCI precursor is more abundant in Sample-1, indicating Sample-1 is more aqueously altered than Sapple-2 (the distance between Sample-1 and -2 is ~1 mm). The most anhydrous region is the chondrule rim. However, the mesostasis of chondrule is aqueously altered. The presence of gypsum indicates strong aqueous alteration although amorphous silicate containing abundant tiny Fe sulfide and Ni-rich metal and enstatite whiskers remains. These features may suggest that some of aqueous alteration in this meteorite occurred in the primitive solar nebula [12]. We found candidates for carbon-rich objects ~1 μm in size and further study is needed by TEM.

The present results strongly suggest that this technique is very useful for initial analysis of Ryugu samples in Hayabusa-2 mission.

References: [1] Greshake A. (1997) *GCA*, *61*, 437-452. [2] Grossman J.N. and Brearley A.J. (2005) *MAPS*, *40*, 87–122. [3] Leroux H. et al. (2015) *GCA*, *170*, 247-265. [4] Kimura M. et al. (2019) *MAPS, 32,* #6042. [5] Matsumoto M. et al. (2019) *Science Advanced. 5*, eaax5078. [6] Nittler L.R. et al. (2019) *Nature Astronomy*. [7] Tsuchiyama A. et al. (2013) *GCA*, *116*, 5-16. [8] Takeuchi A. (2013) *J. Synchrotron Rad.*, *20*, 793-800. [9] Tsuchiyama A. (2017) *LPSC 48,* Abstract #2680. [10] Noguchi T. (2020) *LPSC 51*, this volume. [12] Metzler K. et al. (1992) *GCA 56*, 2873-2897